SSRG International Journal of VLSI and Signal Processing
ISSN: 2394–2584 / https://doi.org/10.14445/23942584/IJVSP-V12I2P102

Volume 12 Issue 2, 9-27, May-Aug 2025

Original Article

Design of a Data Acquisition System and Analysis of Vibration Signals on Helicopters

Sinan Akbaş[1], Selda Güney[2]

[1,2]*Department of Electrical and Electronics, Baskent University, Ankara, Turkey.*

[1]*Corresponding Author : akbas.sinan.01@gmail.com*

Received: 04 June 2025 Revised: 06 July 2025 Accepted: 29 July 2025 Published: 14 August 2025

Abstract - *Health and monitoring of aircraft vibrations are crucial to safety. To maintain safe flying, helicopter vibration levels should be kept at a minimum. Therefore, vibration signal analysis and systems that measure vibration levels are very important topics in the avionics industry.*

In the scope of this thesis, the Flight Test Instrument (FTI) system is designed for data acquisition purposes. The FTI system consists of a power module, controller module, analog input module and backplane module. The power module converts input power to desired levels according to system requirements. The controller module is responsible for calculations and communication because it has an FPGA on board. The analog input module is responsible for interfacing with the sensors, signal conditioning, and sampling the vibration signals. The backplane is designed to combine all the modules together.

The study also contains vibration signal analysis. In order to determine the vibration level and phase, different approaches were made. First of all, to determine vibration magnitude, an FFT implementation was made, and for the phase calculation, several digital filters were designed and implemented into the system. Algorithms that are developed have been verified in laboratory environments with a constant vibration generator device; measurements from a helicopter were taken to measure the vibration level. A commercial off-the-shelf (COTS) device was used in helicopter experiments to compare the results, and the results and comparisons have been shared. Afterwards, several machine learning algorithms (such as SVM, GPR, linear regression, etc.) are trained for vibration magnitude and phase prediction. Simulation results have been shared and evaluated for these algorithms.

Keywords - *Signal Processing, Machine Learning, Hardware Design, Flight Test Instrument, Vibration Signals.*

1. Introduction

The mechanical phenomena known as vibration are defined by oscillatory motion around an equilibrium position or reference point. It is produced by repeatedly moving an object or system back and forth around a central axis or point. This motion can take many different shapes, such as rotational (circular), linear (straight-line), or a mix of the two. Depending on the type of system producing the vibration, it can manifest in a variety of frequencies, amplitudes, and directions. It may be brought on by interactions between system components, internal mechanical or structural characteristics, or external forces operating on a system.

Because vibration has a significant impact on the performance, stability, and dependability of mechanical systems, it is a topic of much research in both engineering and physics. Depending on the situation, it can have both positive and negative impacts. FTI (Flight Test Instruments) systems are basically measurement and data acquisition devices that are used in avionic vehicles.

The main purpose of these systems is to monitor and record specific data in production, maintenance and repair processes. In order to do so, FTI systems contain many transducers, such as air pressure sensors, velocimeters, accelerometers, fuel pressure sensors, cameras, etc.

In engineering and physics, vibration is studied extensively because the performance, stability, and reliability of mechanical systems are affected enormously by vibration. It can have both beneficial and detrimental effects depending on the context [1]:

- Beneficial Effects: In some cases, controlled vibration is desirable and can serve useful purposes. For example, vibration is utilized in machinery such as engines,

turbines, and pumps to facilitate proper functioning, enhance efficiency, and prevent stalling or resonance.

- Detrimental Effects: Excessive or uncontrolled vibration can be problematic and lead to various issues, including mechanical wear, fatigue, instability, and structural damage. In aerospace, automotive, and manufacturing applications, minimizing unwanted vibration is crucial for equipment safety, performance, and longevity.

Understanding the causes and characteristics of vibration, as well as techniques for its analysis, control, and mitigation, is essential for engineers and designers across numerous industries to ensure the reliability and efficiency of mechanical systems [2].

The long-term negative impact of vibration on machines can be significant and can lead to several detrimental consequences, including;

- Mechanical Wear and Fatigue: The wear and tear of machine components such as bearings, gears, shafts, and other moving parts can be accelerated by continuous vibration. This mechanical wear can lead to increased friction, surface damage, and ultimately, component failure due to fatigue.
- Reduced Operational Life Span: The cumulative effects of vibration-induced wear and fatigue can significantly shorten the operational lifespan of machines. Components may fail prematurely, necessitating frequent repairs or replacements, which can increase maintenance costs and downtime.
- Decreased Efficiency and Performance: Vibrations can impair the efficiency and performance of machines by causing misalignments, imbalances, and loss of precision in moving parts. This can lead to decreased productivity, energy inefficiency, and compromised output quality in manufacturing processes.
- Structural Damage and Deterioration: Excessive vibration can cause structural damage to machine frames, housings, and support structures. Over time, this can lead to cracks, deformation, or other forms of deterioration, compromising the overall integrity and safety of the equipment.
- Safety Hazards: Vibrations can create safety hazards for operators and nearby personnel, particularly in high-risk environments such as construction sites, industrial facilities, or transportation vehicles. Uncontrolled vibration can cause machinery to malfunction, leading to accidents, injuries, or even fatalities.
- Environmental Impacts: Vibrations transmitted through the ground or surrounding structures can also have environmental impacts, such as noise pollution or structural vibrations that affect nearby buildings or infrastructure.
- Increased Maintenance Costs: Dealing with the consequences of vibration-related damage requires regular maintenance, inspections, and repairs, all of which incur additional costs for equipment owners and operators. Addressing vibration issues proactively through preventive maintenance measures can help mitigate these costs in the long run.

Overall, the long-term negative impact of vibration on machines underscores the importance of implementing effective vibration monitoring, control, and mitigation strategies to maintain equipment reliability, safety, and longevity.

This includes measures such as proper machine design, maintenance of optimal operating conditions, periodic inspections, and the use of vibration isolation or damping techniques where applicable.

The main compound of the FTI system is the data acquisition unit. This part of the system contains a lot of analog circuitry and ADC channels in order to sample and monitor the desired data. Therefore, in DAQ units, several types of signal conditioning and filtering circuitries exist for each type of sensor. After the desired data is conditioned and sampled by analog circuitry, it is fed through to the digital part of the system, which is the controller unit of the FTI system.

The controller unit of the system mostly contains FPGA-based designs, but when the older designs are analyzed, one can see that it was common to use MCU-based controller designs. The last but essential part of the FTI System is the Power modules. All the transducers, sensors, DAQ modules, and controller units require different power supplies to perform their duties. The avionic vehicle environment is very noisy due to the complex devices and mechanical structures.

FTI power modules are obligated to supply clean power to the other compound of the FTI systems [3]. In the concept of study, an FTI system consisting of a power module, analog input module, controller module and backplane module to bring them all together is designed. Afterwards, signal processing algorithms for vibration level and phase detection are developed and implemented in the designed system.

Finally, machine learning algorithms are used in the MATLAB environment in order to compare with the signal processing algorithms. A comparison is made using evaluation metrics such as RMS, MSE, and MAE.

2. Materials and Methods

2.1. Power Module Design

Before designing the power module of the FTI system, the power requirements of the entire system are listed. Then, the power design was conducted and implemented. Power requirement of the system can be summarized as follows;

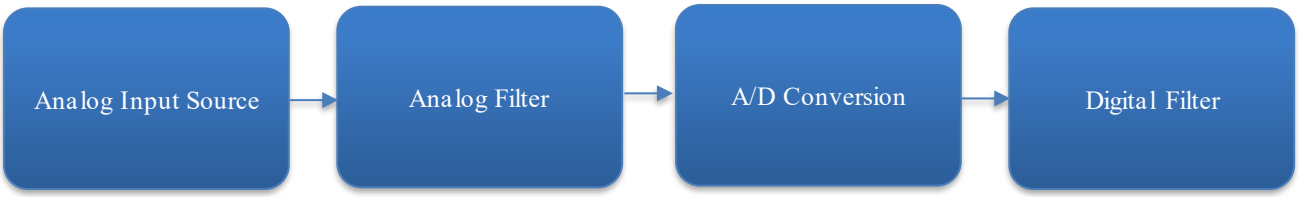

Fig. 1 Data flow chart

- 1500V isolation voltage
- 1000 Mohm isolation resistance
- -40/+85 oC working temperature
- +15V +/- 100mVp-p ripple, 0.5A output
- -15V +/- 100mVp-p ripple, 0.5A output
- +12V +/- 100mVp-p ripple, 0.5A output
- -12V +/- 100mVp-p ripple, 0.5A output
- +5V +/- 75mVp-p ripple, 4A output
- Overvoltage protection
- Overcurrent protection
- 18 – 40 VDC input voltage range

In order to meet the criteria, Traco Power TEN20WIN series of DC/DC converters are used and implemented in the power module of the system. TEN20WIN has various output voltage levels and is appropriate for rugged military designs. A number of crucial features of the DC/DC converter are listed below [4];

- 18 – 75 VDC input voltage range
- 3.3 VDC, 5VDC, 12VDC, 15VDC, -5VDC, -12VDC, -15VDC output
- Efficiency between 85-89%
- 5VDC 4A output capacity
- +15V 667mA capacity
- -15V 667mA capacity
- +12V 883mA capacity
- -12V 883mA capacity
- -40 to +85 oC operating temperature
- MIL-STD 810F compliance
- 27g weight

2.2. Analog Input Module Design

In order to design an anti-aliasing filter, we should know the frequency region in which we are interested. Due to the rpm of both main and tail rotors, the maximum frequency we would like to deal with is no more than 10kHz. (For this reason, in section 3.2.ADC Block, Nyquist Frequency and ADC selection are given in detail. Of course, in different applications, the frequency region of interest can vary due to the requirements of the system.

Analog filters can be used for different applications such as pre-amplification, equalization, tone control, tuning and preventing the aliasing for out of the frequency region of interest for digital signal processing applications. For data acquisition systems, the general signal flow can be expressed in Figure 1.

Butterworth filter is best suited for a data acquisition system that is designed. Since the vibration magnitude detection is done using the velocimeter signal's amplitude, a flat bandpass response of filters is chosen to simplify the design and calculations. An anti-aliasing filter can be designed after the bandpass region is determined to be 10 kHz. Before getting to the design stage, it is also known that helicopters and other aviation crafts are very noisy environments in terms of both electrical and mechanical aspects. That is why we would like to design an anti-aliasing filter roll with a very sharp roll-off. That is why the Butterworth lowpass filter with 10kHz cutoff, stop band at 20kHz with a 60dB gain is designed.

The reason for the selection of the Butterworth filter topology is the flat bandpass response. Since the magnitude estimation is crucial for the vibration magnitude of the system, a gain change in the bandpass region is not wanted. Therefore, a 0 dB gain with a flat bandpass response Butterworth filter is designed as follows. In order to achieve filter characteristics, a 10th-order 5-stage Butterworth lowpass filter has been used. The circuitry is given below in Figure 2.

The magnitude response of the designed Butterworth filter is given below in Figure 3 [5];

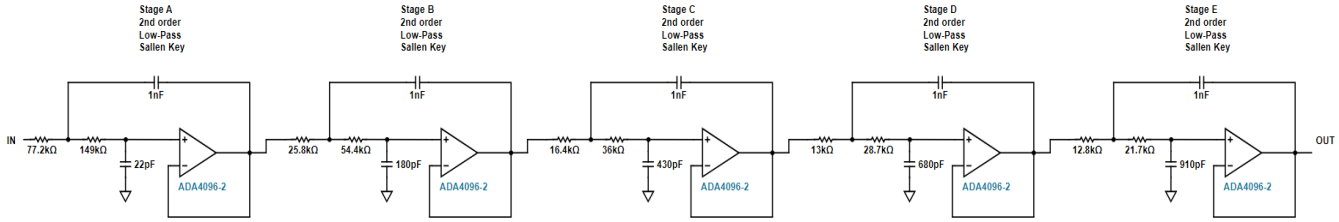

Fig. 2 Designed 10th Order 5 Stage Butterworth Low Pass Filter with 10kHz Cut off, stop band at 20kHz with a -60dB gain

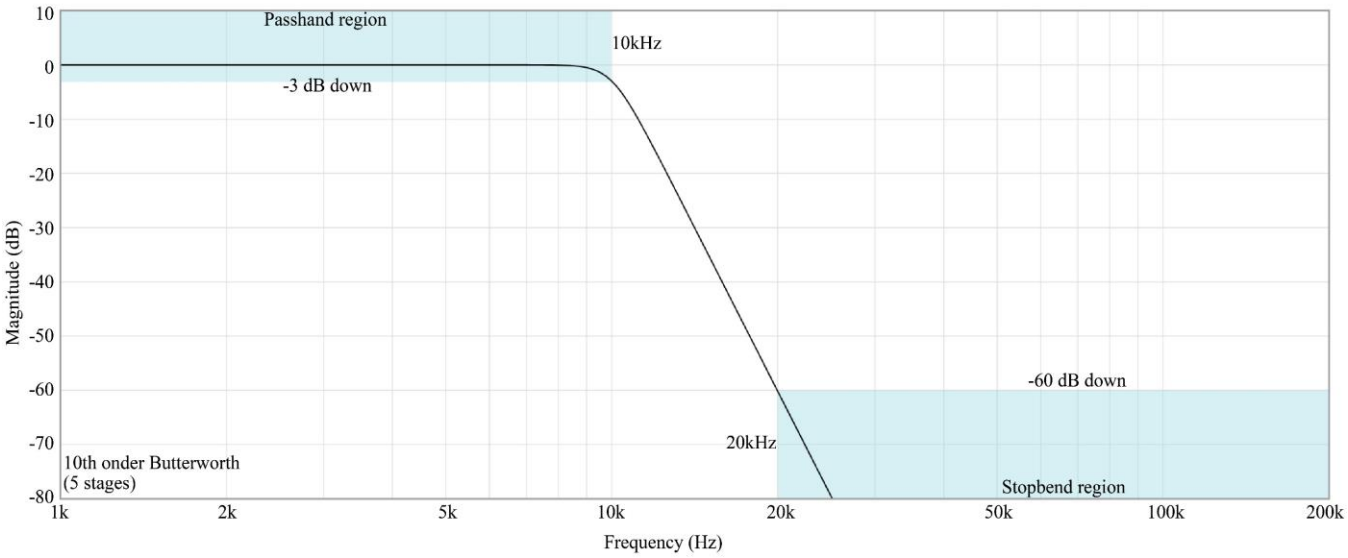

Fig. 3 Magnitude Response of Designed Butterworth Filter

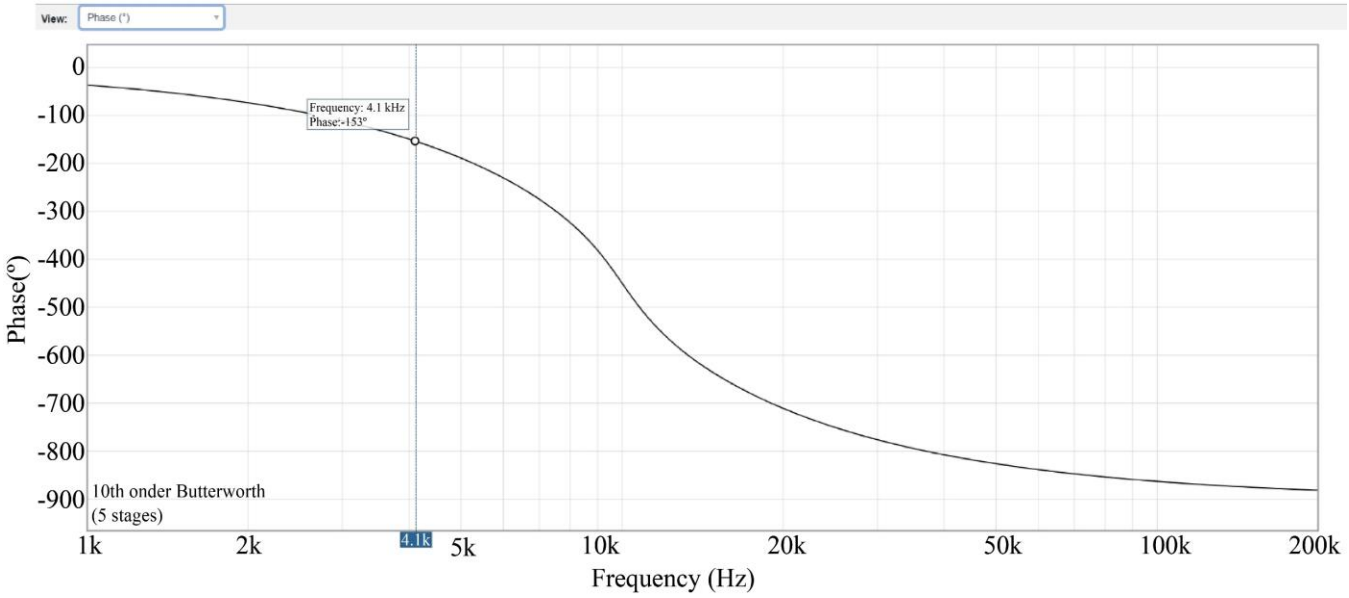

Fig. 4 Phase Response of Designed Butterworth Filter

In our application, a sigma-delta type ADC is preferred. Since the output of the velocimeter sensor is in the range of millivolts, the data acquisition system needs higher resolution, and, of course, one can know that aircrafts are very noisy environments both electronically and mechanically. Due to defining these design constraints and determining the desired region of frequency, ADC with a manufacturing part number ADS1278 is chosen.

ADS1278 is an excellent choice for our design due to several reasons. Such as: It has simultaneous sampling capability up to 8 channels, 144kSPS data rate, which is more than enough for the Nyquist frequency, very high signal to noise ratio (111dB), SPI data interface, and differential analog input that is resilient to common mode noise.

Due to the analog input ranges of the ADS1278, the input signal range of the system is -2.5V to +2.5V. Since the velocimeter output is single-ended and the inputs of ADS1278 are differential-ended, a single-ended to differential-ended converter op-amp is used. For this purpose, the OPA1632 differential amplifier is used. The reason for the selection of OPA1632 is that it has a very wide supply range (+/- 15V), and it is recommended in the ADS1278 datasheet for a compatible input type. For the voltage reference (VREFP) of the ADS1278, the voltage reference IC REF5025 is used. Privileges of the voltage reference ICs can be summarized as follows;

- Very low output noise
- Very high precision output voltage accuracy
- Very low drift

Since ADC's performance depends upon its voltage reference, using low-noise and high-precision voltage reference ICs is wise.

Due to its stable passband response, ADS1278 is configured for high-resolution mode in this design. The response is given below [6].

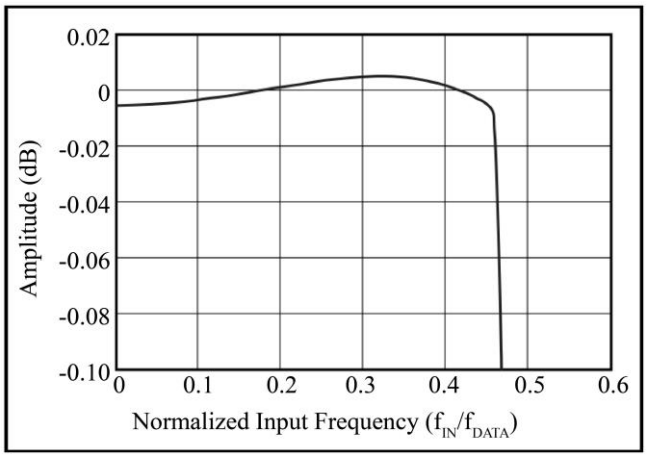

Fig. 5 Passband Response of ADS1278

In order to configure ADS1278 for high resolution mode, MODE[1:0] pins are set to '01', clock frequency is set to 27MHz, and the sample rate of the ADS1278 is set to 52.734 KSPS. For the digital output of the ADS1278, FORMAT[2:0] pins are set to '001' for SPI interface and fixed TDM data output mode, meaning that, at the first DOUT1 pin of ADS1278, sampled data are fed through in channel order (i.e. CH1, CH2, CH3, etc.). The representative figure is shown below.

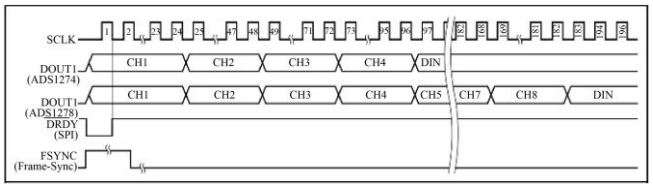

Fig. 6 TDM Mode All Channels Enabled

In this design, an FPGA of the Zynq 7015 family has been used to collect sampled data from the ADC. The selected Zynq-7015 is in the SoC (system on Chip) family, unlike the FPGAs. SoCs consist of PL (Programmable Logic) and PS (Processing System). The PL side is an FPGA part, and the working principle is identical to that of FPGAs. The PS side can be considered an ARM-based MCU (Micro Controller Unit), and the working principle is the same as that of MCUs. In order to program the PS side, the C language can be used. Since the ADS1278 has an SPI interface, an SPI communication module is designed in VHDL to configure the ADS1278 and also for data collection. In order to boot the FPGA and keep the relevant data for the algorithm, a QSPI and an EEPROM IC are included in the design. Also, for the communication between the Analog Input Module and Controller Module, AXI Quad SPI IP is used.

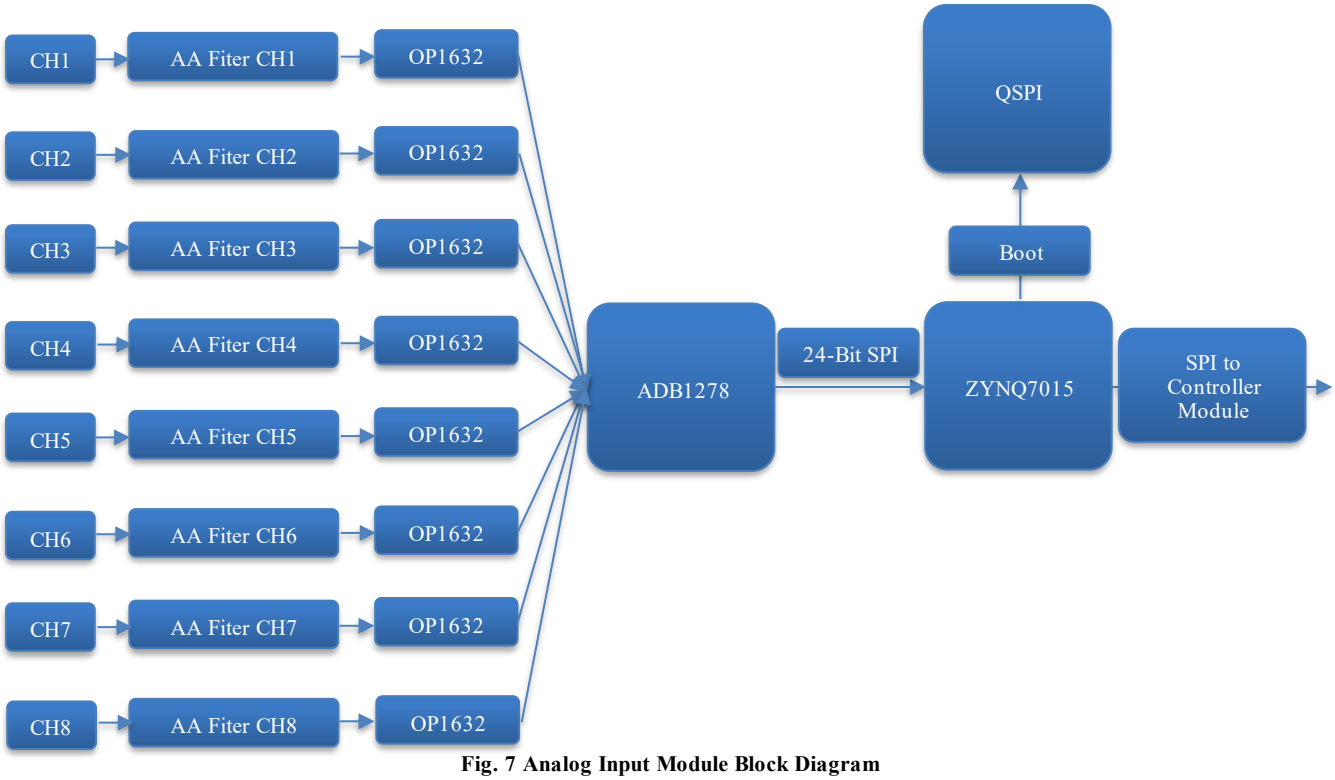

Fig. 7 Analog Input Module Block Diagram

The overall block diagram of the analog input module is given in Figure 7. The specifications of the designed Analog Input Module can be summarized as follows;

- 8 simultaneous analog input channels
- Up to 144 kSPS data rate
- +/- 2.5V input range
- Lowpass filter with a cutoff of 10 kHz
- 0.298 uV resolution
- 15.6 uIPS vibration measurement resolution

2.3. Controller Design

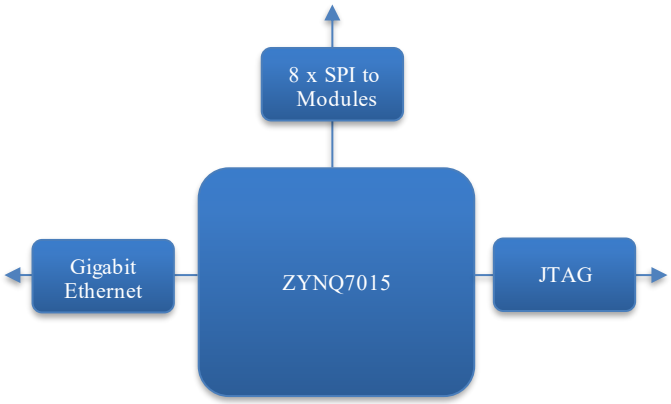

Fig. 8 Block Diagram of Communication Interfaces

This design implements a Gigabit Ethernet communication interface to link the designed DAQ device to the user's PC. As one knows, an Ethernet interface is very common and is available on many current computers. Moreover, since the gigabit Ethernet is backwards compatible, meaning that it can work as 100-base or 10-base, the gigabit Ethernet selection is efficient for this design. The Marvell 88E1512 PHY with RGMII interface has been chosen for the physical layer. The RGMII interface has 4 data lanes and one control and clock lane for each transmit and receive side.

88E1512 integrated circuit converts RGMII interface to Ethernet interface. In a gigabit Ethernet interface, there are four differential lanes (MDI[0], MDI[1], MDI[2], MDI[3]). These data lanes can be routed to an RJ45 Ethernet connector or different high-speed connectors to connect Ethernet data lines. During the design phase, the hardware designer should pay attention to matching the lengths of receiver and transceiver traces of RGMII signals individually. The MDI signals should also be matched. Length matching issue is crucial for high-speed interfaces because the travelling time or delay time for each data lane should be equal. If the mismatch occurs between the lanes, then the communication interface cannot be established due to a design failure. The overall block diagram of the Ethernet is given below;

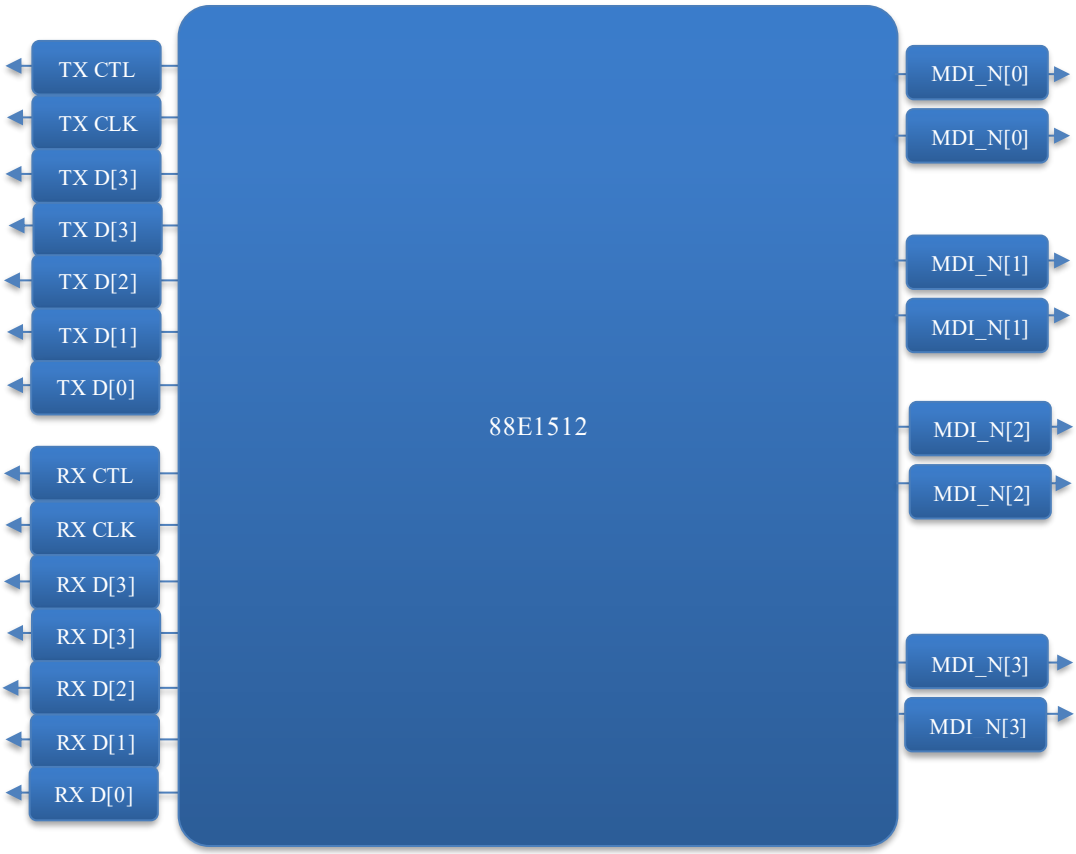

Fig. 9 Block Diagram of Ethernet Interface

After clarifying the hardware side of the Ethernet protocol, IPv4 is used for the embedded side. The IwIP is a TCP/IP Ethernet protocol implementation found in Vitis IDE (Integrated Development Environment), a development tool AMD provides for PS side implementations. Usage efficiency and availability of the IWIP are considered; many embedded designers are using IWIP for Ethernet application implementations.

This design used examples of lwIP echo server application codes to construct the system's Ethernet communication. The controller module is getting data from analog modules, then processing with DSP operations and algorithms, sending the output of the processed sensor data to the host pc through an Ethernet interface. A colleague of mine conducted the embedded design of the system. The overall data flow representation is given below.

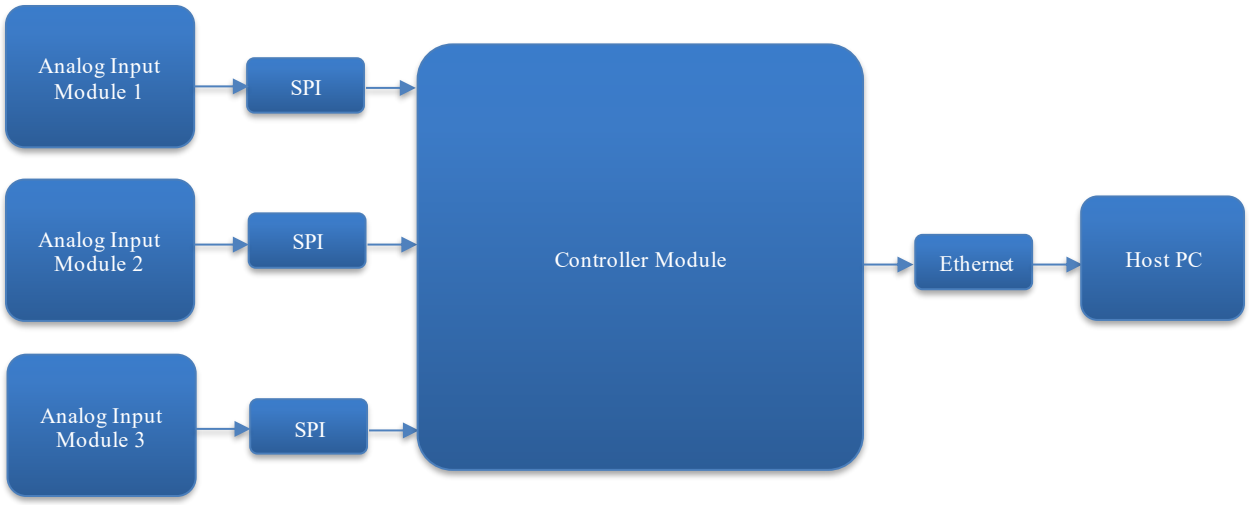

Fig. 10 Communication Data Flow Chart Between the Modules and Host PC

2.4. Sigal Processing Algorithms

In order to make it clearer, the sensor types that are used in the system and their functions should be mentioned. A magnetic pick-up sensor for tracking the rotation of the main rotor is used. A magnetic pick-up sensor produces a sine wave output whenever a change from a non-magnetic material to a magnetic material occurs. Since the vibration signals are periodic due to the rotation of the helicopter blades, it is essential to track the period start time of the rotation of the blade. Helicopters can have more than two blades. Independent of the number of blades, one blade is chosen as the target blade, and the target blade has a magnetic metal extension at the main rotor side of the target blade that can trigger the magnetic pick-up sensor mounted on the helicopter's main rotor. Since the blades' rotational motion is 360, the front of the helicopter is accepted as 0. Whenever the target blade flies through the front of the helicopter, the magnetic pick-up sensor produces a sine wave-shaped signal. Therefore, the time period of vibration signals is determined. During these sinus peaks, vibration signals are sampled and processed.

The main vibration source in helicopters is the main rotor due to the large and heavy rotating blades. The RPM value can change according to the helicopter type; however, in this study, the helicopter that is used rotates at 324 RPM. Large and heavy rotating blades create vibration on the aircraft vertically and horizontally. In order to sense vibrations, two velocimeter sensors are used for both the x-axis and y-axis. Velocimeters are mounted inside the helicopter horizontally and vertically, respectively. While a horizontally mounted velocimeter detects horizontal vibration, a vertically mounted velocimeter detects vertical vibration. These velocimeters need +12V and 12V supplies and produce a very noisy sinusoidal vibration signal. While the amplitude of the output of the velocimeter sensor defines the vibration magnitude, the phase of the signal with respect to the magnetic pick-up sensor defines the vibration location. In light of this information, the sampling start of the velocimeter signals is triggered by a magnetic pick-up signal.

IPS (inch per second) is a unit of measurement that is used to define the velocity of a vibration. Since the output of the velocimeter is sinusoidal, the conversion between the sinusoidal signal's amplitude and IPS is defined in the velocimeter datasheet as 1 IPS = 19mV. Therefore, vibration magnitude is given in IPS.

In this design, FFT is used to determine the magnitude of the vibration level. In order to test the algorithm, a device that can produce a constant vibration is used. This device produces a vibration at 0.4 IPS (+/- 0.04 IPS), 275 (+/- 15 °), and also a velocimeter and magnetic pick-up can be mounted on the device in order to get a vibration signal, and the device rotates at 15 Hz, meaning that the vibration signal is expected at 15 Hz.

A size of 1024 (N=1024) time series samples is used for FFT calculations. Since the ADC's sample rate is 52.734 kSPS and the used lab device is generating a vibration signal at 15Hz, 52.734 kSPS is unnecessary. Therefore, the decimation technique is used to simplify the calculations. After the decimation, a 1024-point FFT is performed in MATLAB. The plotted raw data of the vibration signal of the test device is given below;

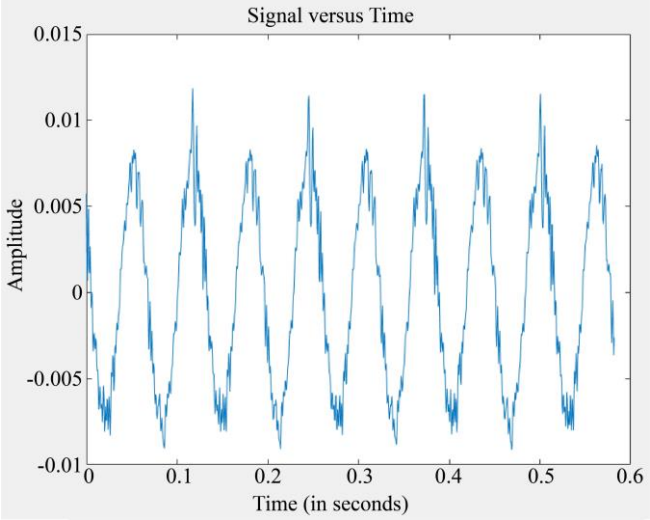

Fig. 11 Raw Data of the Vibration Signal

After taking the FFT of the raw data, the vibration signal in the frequency domain can be seen as follows;

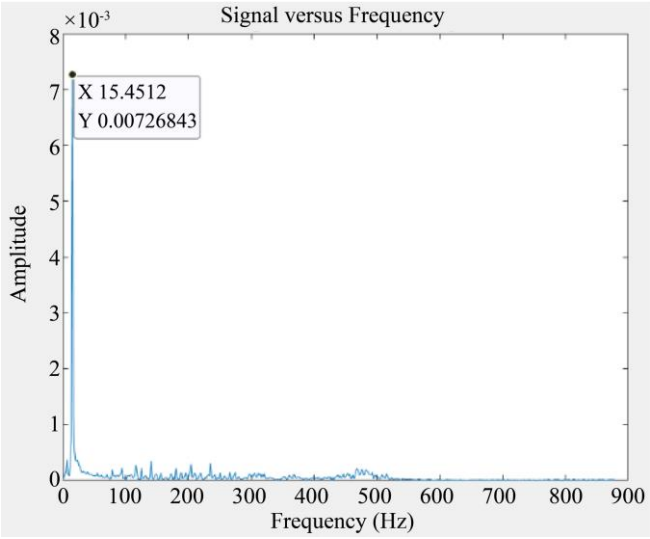

Fig. 12 Vibration Signal in Frequency Domain

As mentioned before, after taking the FFT of the signal, a peak is detected at 15 Hz as expected, with a magnitude of 7.26843 mV. Since 19 mV is equal to 1 IPS, then 7.26843 mV / 19 mV = 0.3825 IPS. This also shows that both the measurement and the calculation of the vibration level are consistent because these studies are done due to a constant vibration-producing device.

After determining the vibration magnitude, the phase of the vibration signal should be determined. Since the output of the velocimeter signal is noisy, calculating the phase is challenging. In order to eliminate this problem, a digital filter should be applied to the signal to eliminate the noise from the vibration signal. The MATLAB tool Filter Designer is used to design a digital filter because it is very efficient for designing a filter with different parameters and simulating the filter in the MATLAB environment.

With the Filter Designer tool, an FIR equiripple lowpass filter is designed with a cutoff frequency at 0.08 normalized frequency and a stopband normalized frequency at 0.12. Gain ripple in the passband region is set to 0.01 dB, and stopband attenuation gain is set to -100 dB for better performance. As a result of these parameters, a 236th-order lowpass FIR filter is implemented in the phase detection algorithm.

The magnitude response of the FIR filter is shown below. As one can see from the figure, the filter has a very flat passband response, and the filter's roll-off is very sharp due to adjusted filter parameters.

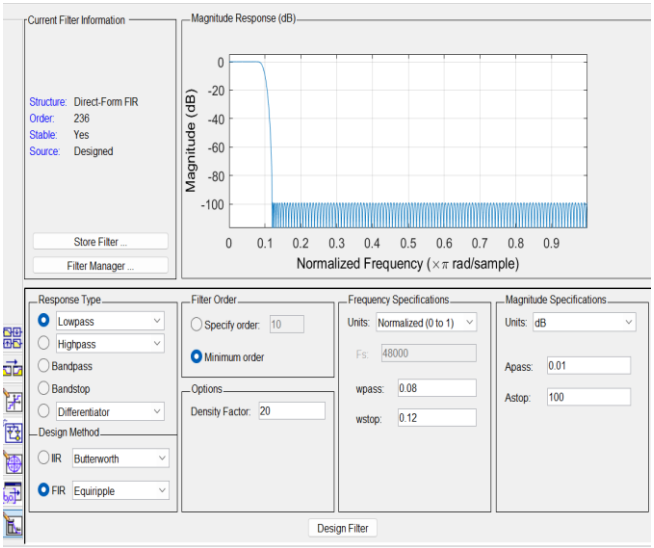

Fig. 13 Magnitude Response of Digital Lowpass Filter

Conversion between the frequency and the normalized frequency can be done through the following formula;

$$\text{Normalized Frequency (in rad/sample)} = (f \times 2\pi) / \text{Sampling Frequency}$$

In this design, decimation is set to 30 for sampling the velocimeter output, resulting in a sampling frequency of 1757 SPS (i.e. 52734/30 = 1757). After calculating the frequency using the new sampling frequency, the approximately filter has a cutoff frequency at 22 Hz and a stopband frequency at 33 Hz. Since the interested signal is at 15 Hz, this filter works very efficiently for this application. The designed filter's group delay (in samples) is shown below.

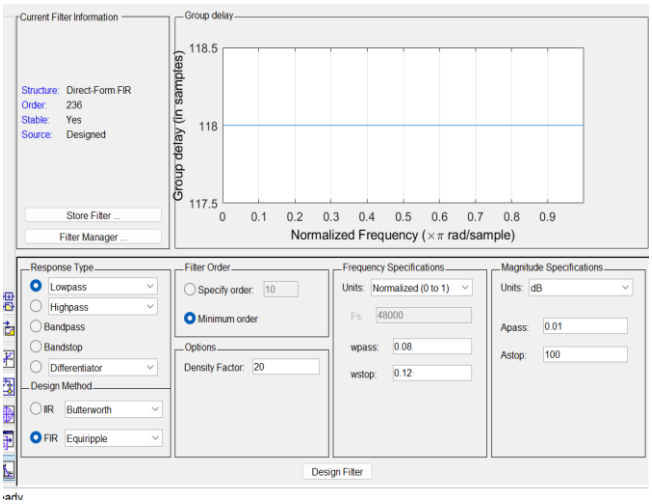

Fig. 14 Group Delay of Digital Lowpass Filter

After applying the lowpass filter to the raw velocimeter signal, the filtered signal is given below. As one can see, the filtered vibration signal is almost a pure sinusoid after removing the noisy components of the signal.

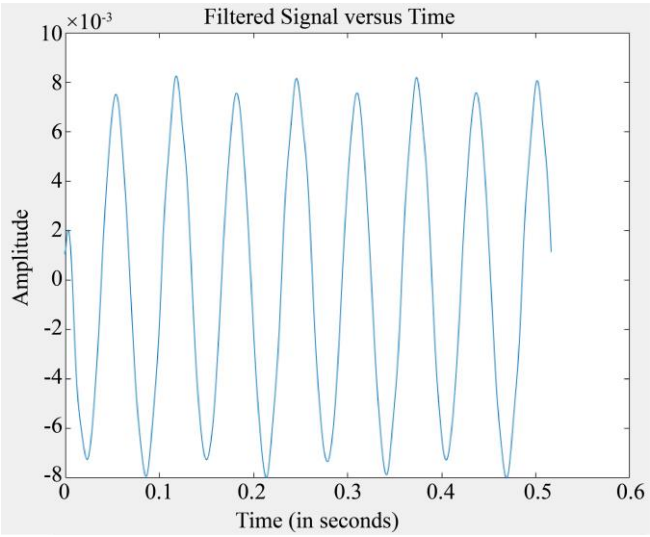

Fig. 15 Filtered Signal

After getting the filtered data, the phase of the vibration signal can be calculated. Group delay of digital lowpass filter, group delay of ADC, because sigma-delta ADC also have an embedded digital filter in it and also phase response of anti-aliasing analog filter is taken into account, the phase of the vibration signal with respect to the magnetic pick-up sensor can be calculated.

When calculating the phase of the vibration signal, the time domain filtered signal sampled with respect to the peak value of the magnetic pick-up sensor is used. Due to this triggered sampling technique, converting the first peak of the vibration signal's time value to phase in terms of degrees, one can get the phase of the vibration signal.

After verifying the algorithm with a laboratory setup, measurements were made on a helicopter. Of course, the digital filter had gone through a few modifications with respect to the change of the vibration frequency. However, as can be seen from the figure below, raw velocimeter data on a helicopter is noisier than the laboratory setup, as expected due to the noisy nature of aircraft, both mechanically and electronically.

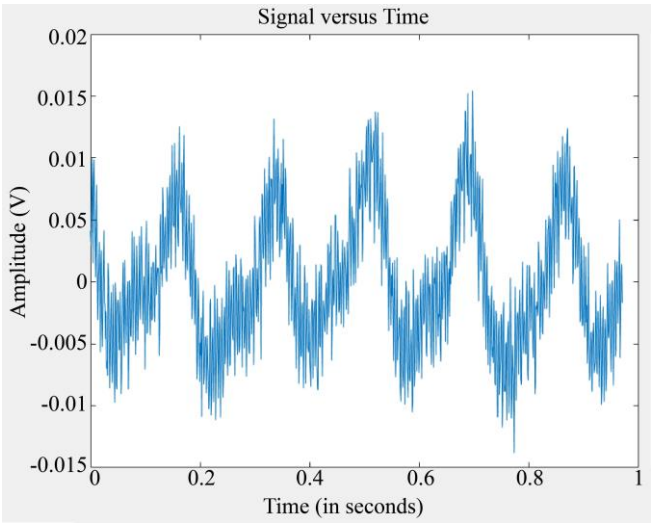

Fig. 16 Velocimeter Raw Data Taken from Helicopter

Since the subject aircraft for the study has a constant 324 RPM main rotor blade rotation speed, meaning that a 5.4 Hz frequency, the filter characteristics have been changed according to the application. For the causation of the noisy environment, a bandpass filter with a very sharp and narrow bandwidth had been designed with cutoff frequencies at 5.2 Hz and 6 Hz. Moreover, band-stop frequencies of the filter had been set to 3 and 10, respectively. The magnitude response of the designed filter is shown below.

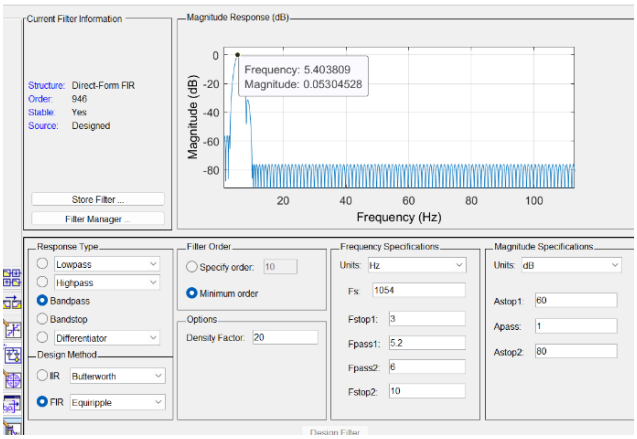

Fig. 17 Designed Digital Bandpass Filter for Helicopter

As the sharpness increases and the bandwidth decreases, the order of the filter increases as expected. Due to these specifications, the group delay increases. After applying the

new filter for the raw data of the velocimeter, which is taken from the aircraft, the filtered signal becomes as follows.

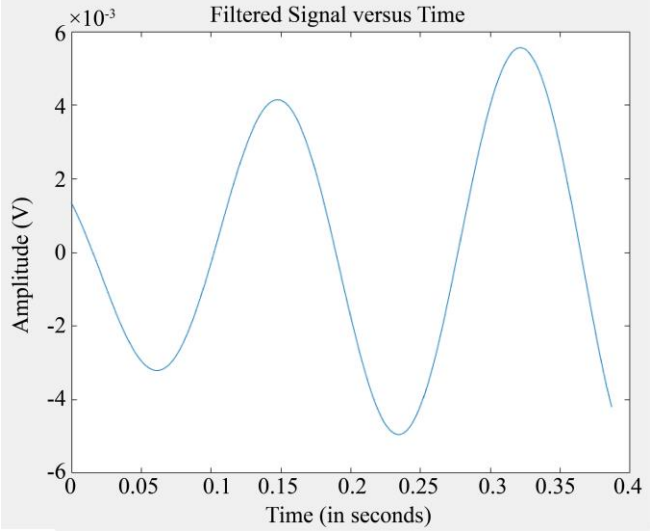

Fig. 18 Filtered Vibration Signal of Helicopter

The vibration magnitude of the aircraft is identical to the laboratory study; taking the FFT of the signal shows a peak at 324 RPM or 5.4 Hz. The result of the FFT calculation of the aircraft velocimeter can be seen below. As a result, vibration magnitude is measured as approximately 0.2 IPS.

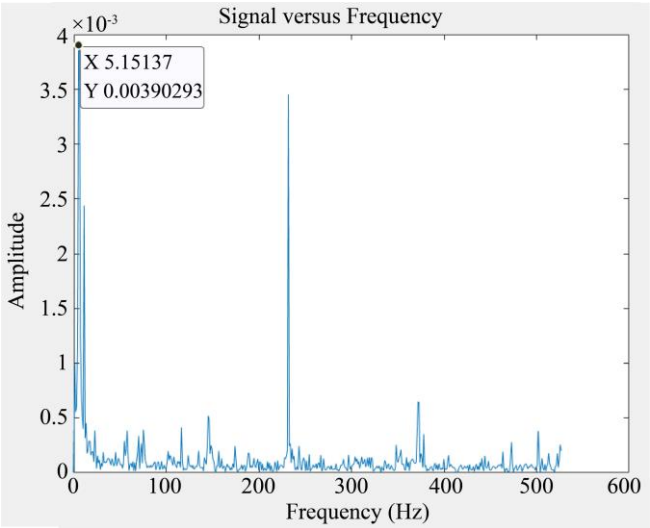

Fig. 19 FFT Plot of Aircraft Measurement

Of course, both in a laboratory environment and in aircraft, lots of measurements are taken. A comparison of these measurements and methods will be reviewed in the Discussion and Results section.

2.5. Regression Methods

This part of the paper describes another approach for estimating the vibration levels due to sampled vibration signals. As an alternative to signal processing algorithms, a regression model-based approach was implemented in MATLAB. In order to do so, lots of measurements are taken from both the constant vibration generator lab device and the helicopter. Afterwards, these measurements are used to train the regression models to estimate the vibration level and phase more accurately. The algorithms that predict the vibration magnitude and phase better are Support Vector Machine (SVM), Decision Trees, Gaussian Process Regression and Ensemble Learning. Then, these models were compared according to evaluation metrics. The evaluation metrics that are used in this study are Mean Squared Error (MSE), Root Mean Square Error (RMSE) and Mean Absolute Error (MAE).

2.5.1. Support Vector Machine (SVM)

Support Vector Machine is a machine learning algorithm defined as a set of related supervised learning methods. This algorithm is usually used for regression and classification. The advantages of SVM can be considered as the training algorithm is convenient because it is not locally optimal. Also, SVM can be scaled for high-dimensional data. SVM algorithms require a good kernel function, which can be considered a disadvantage [9].

2.5.2. Decision Trees

Decision tree learning is a machine learning algorithm that is a type of supervised learning. In order to predict the outcome, regression decision trees can be used as predictive models. Decision trees are commonly used in machine learning applications to predict the target value by using a set of input data. The key feature of decision trees is a recursive segmentation of a target data field based on the values of related input fields or indicators to form divisions, along with related descendant data segments (referred to as leaves or nodes), that include progressively comparable intra-leaf objective values and gradually varying inter-leaf at specific level of the tree [10].

2.5.3. Gaussian Process Regression

A Gaussian process is known as a stochastic process in probability and statistics theory, meaning that variables collected or sampled randomly are indexed by time or space. In order to infer the best possible output from a given data set, a Gaussian process regression model can be used as an efficient algorithm. Gaussian process regression can be defined as a non-parametric Bayesian approach, meaning that by using a theoretically limitless number of parameters and allowing the data to determine the amount of complexity through the use of Bayesian inference, it may capture a wide range of links between inputs and outputs [11].

2.5.4. Ensemble Learning

An ensemble learning method depends on using multiple learning algorithms in order to give better predictions. In the simulation, the bagged trees approach was revealed to have

better performance. Bagging method can be considered as the first ensemble learning method and is reviewed as one of the simplest ensemble learning methods. The technique employs bootstrapping or sampling with a replacement method to use several versions of a training set. A distinct model is trained using each of these data sets. The aim is to produce a single output; the model outputs are aggregated by voting (for classification) or averaging (for regression) [12].

2.5.5. Mean Square Error (MSE)

Mean square error can be described as the signal's similarity or discrepancy/variations. Therefore, one signal is commonly assumed to be the original signal, and the other is assumed to be a distorted or noisy signal. Then the MSE of the signals can be defined as follows;

$$MSE(x,y) = \frac{1}{N}\sum_{i=1}^{N}(x_i - y_i)^2 \quad (1)$$

Where x and y are two finite discrete signals with a sample size of N.

Generally, ei is defined as the error signal and equals the subtraction of x and y signals.

$$ei = xi - yi \quad (2)$$

Then, the formula of the MSE becomes as follows [7];

$$MSE(x,y) = \frac{1}{N}\sum_{i=1}^{N}(e_i)^2 \quad (3)$$

2.5.6. Root Mean Square Error (RMSE)

The idea behind the root mean square error is that it is the quadratic mean of the error signal (i.e. ei). By this methodology, the accuracy of the model can be measured. The following formula expresses the RMSE,

$$RMSE = \sqrt{\frac{1}{N}\sum_{i=1}^{N}(x_i - y_i)^2} = \sqrt{\frac{1}{N}\sum_{i=1}^{N}(e_i)^2} \quad (4)$$

Where x and y are two finite discrete signals with a sample size of N, and ei is the error signal, which equals the subtraction of the x and y signals [8].

$$ei = xi - yi \quad (5)$$

2.5.7. Mean Absolute Error (MAE)

Similar to MSE and RMSE, mean absolute error can be described as the sum of absolute errors divided by sample size N. It is an alternative to MSE and RMSE, and the formula for MAE is given below;

$$MAE(x,y) = \frac{1}{N}\sum_{i=1}^{N}|x_i - y_i| = \frac{1}{N}\sum_{i=1}^{N}|e_i| \quad (6)$$

Where x and y are two finite discrete signals with a sample size of N, and ei is defined as the error signal, equal to the subtraction of the x and y signals.

$$ei = xi - yi \quad (7)$$

These defined evaluation metrics are used to compare the machine learning algorithms. Successful algorithms observed in the "Regression Learner" MATLAB Module are: Support Vector Machine (SVM), Tree, Gaussian Process Regression, Ensemble and Kernel.

2.6. Experimental Studies

Within the scope of this study, an FTI system is designed for vibration signal measurement on helicopters. Then, a signal processing algorithm is developed and implemented in a designed FPGA-based FTI system. The developed algorithm is verified by using a constant vibration generator lab device. As mentioned before, the vibration generator lab device produced a constant 0,4 IPS (+/- 0.04 IPS) vibration at 275 (+/- 15o) phase angle. The measurements taken for verification from the lab device are given below.

Table 1. Vibration Calculations of Measurements of Lab Device

Measurement Number	Vibration Magnitude (in IPS)	Vibration Phase (in Degree)	Measurement Number	Vibration Magnitude (in IPS)	Vibration Phase (in Degree)
1	0.3896	278.0911	36	0.3888	278.5031
2	0.4038	278.2232	37	0.3886	278.5757
3	0.3825	270.1181	38	0.3884	278.911
4	0.3827	270.3766	39	0.3892	279.652
5	0.3827	270.4677	40	0.3906	279.1078
6	0.383	273.3506	41	0.39	277.5953
7	0.3827	270.4677	42	0.387	272.8437
8	0.3838	270.197	43	0.3873	270.6128
9	0.3837	270.8323	44	0.3847	273.4786
10	0.3836	272.3532	45	0.3866	273.4095

11	0.3841	273.0519	46	0.3864	272.4733
12	0.3836	277.266	47	0.3018	286.0034
13	0.3846	268.862	48	0.3899	273.1134
14	0.3843	269.9771	49	0.3893	271.7736
15	0.3844	270.8421	50	0.3893	279.5294
16	0.3852	271.4689	51	0.3872	270.2899
17	0.3848	271.4759	52	0.3902	278.5775
18	0.3847	273.4084	53	0.3851	272.7611
19	0.3845	273.2377	54	0.3893	276.8596
20	0.3855	277.7059	55	0.3867	270.5873
21	0.3861	279.5153	56	0.3894	282.3975
22	0.3869	271.7744	57	0.3853	276.6595
23	0.3873	276.5397	58	0.3865	273.4824
24	0.3866	277.1684	59	0.3859	272.0306
25	0.3872	275.5763	60	0.3933	279.7182
26	0.3875	276.8587	61	0.3858	272.5401
27	0.3876	277.1159	62	0.3884	277.513
28	0.3882	278.6281	63	0.3897	278.0817
29	0.3881	278.9732	64	0.3899	278.5258
30	0.3881	279.2532	65	0.3876	273.3083
31	0.3879	279.2429	66	0.3906	278.3825
32	0.3878	279.4517	67	0.3895	278.6654
33	0.389	276.9816	68	0.3895	282.8705
34	0.3883	277.0849	69	0.3849	270.2137
35	0.3887	277.5389	70	0.3842	273.3562

Measurement Number	**Vibration Magnitude (in IPS)**	**Vibration Phase (in Degree)**	**Measurement Number**	**Vibration Magnitude (in IPS)**	**Vibration Phase (in Degree)**
71	0.3891	276.9226	104	0.389	279.5511
72	0.3884	278.0894	105	0.3821	269.127
73	0.3891	278.7388	106	0.3815	269.2714
74	0.3893	277.8472	107	0.3824	269.4738
75	0.3895	279.2505	108	0.3825	270.4111
76	0.3874	277.2794	109	0.3828	272.1517
77	0.3878	277.6068	110	0.3842	269.757
78	0.3406	294.7666	111	0.3836	270.3909
79	0.3848	271.4057	112	0.3835	270.9227
80	0.3856	270.5173	113	0.384	271.2152
81	0.3883	276.8362	114	0.3836	271.9548
82	0.385	272.6523	115	0.3832	272.5551
83	0.3853	272.231	116	0.3841	272.5441

84	0.3851	273.3062	117	0.3833	273.2305
85	0.3844	273.5137	118	0.3835	273.366
86	0.3891	277.153	119	0.3838	273.5273
87	0.3855	272.8815	120	0.3845	273.5038
88	0.3874	277.8682	121	0.3847	270.5502
89	0.3908	273.3643	122	0.3856	278.7988
90	0.3897	278.3583	123	0.3864	275.6509
91	0.3862	273.3897	124	0.387	276.1907
92	0.3887	277.9743	125	0.387	276.5358
93	0.3837	270.4996	126	0.3871	277.3118
94	0.3866	273.4917	127	0.3872	279.401
95	0.388	276.8798	128	0.3881	276.338
96	0.3861	270.6851	129	0.3875	278.163
97	0.39	277.083	130	0.3875	279.0325
98	0.3852	272.3461	131	0.3879	279.0475
99	0.3849	269.7986	132	0.3879	279.0475
100	0.4352	288.633	133	0.3879	279.0475
101	0.385	273.1626			
102	0.3889	276.9804			
103	0.3856	270.6296			

As shown from the table, all measurement results are in the range of the lab device output, which is between 0,36 IPS – 0,44 IPS and 260o – 290o °. After the designed system is verified using this method, vibration signals on the helicopter will be obtained.

Afterwards, the designed FTI system was mounted to the helicopter, and vibration signal measurements were taken from the helicopter. In order to verify the designed FTI system, another vibration analyzer device is used for control.

The experiment was conducted as follows: firstly, the designed FTI system was mounted on a helicopter, then the helicopter was started to run on the ground at flight RPM. After the flight, RPM was reached by the helicopter engines, vibration measurements were taken through the velocimeter sensors, and vibration measurement results were logged for comparison.

Afterwards, the FTI system is demounted from the helicopter, and the COTS vibration analyzer device is mounted on the helicopter to get the vibration measurement and compare the results. Measurements are taken for both horizontal and vertical vibrations. The result of the measurement and the comparison data of the COTS device is given below;

Table 2. Horizontal Vibration Measurement Taken from Designed FTI System

Measurement Number	Vibration Magnitude (in IPS)	Vibration Phase (in Degree)
1	0.1603	217.51
2	0.2	227.96
3	0.1982	223.34
4	0.1924	238.27
5	0.1664	234.99
6	0.2271	223.45
7	0.1699	204.6
8	0.1777	206.68
9	0.1763	217.72
10	0.1882	225.58
11	0.1355	242.95
12	0.1469	239.12
13	0.1582	222.11
14	0.1602	240.21

Table 3. Horizontal Vibration Measurement Taken from COTS Device

Number	IPS	Phase
1	0.202	260
2	0.257	246

As can be seen from the tables, both the IPS and phase values of the horizontal vibration measurements of both devices are very close. Measurement results of each device were not expected to be exactly the same because the vibration of the helicopter may vary depending on the condition. The following tables show the vertical vibration measurement results. As can be seen from the tables, both IPS and the Phase measurements of the vibration signal are very close to COTS device measurements.

Table 4. Vertical Vibration Measurement Taken from Designed FTI System

Number of measurements	Vibration Magnitude (in IPS)	Vibration Phase (in Degree)
1	0.181	41.28
2	0.172	25.48
3	0.126	48.83
4	0.16	29.58
5	0.23	91.18
6	0.152	64.16
7	0.159	66.79
8	0.117	74.72
9	0.123	51.59
10	0.103	85.98
11	0.136	57.83
12	0.12	64.5

Table 5. Vertical Vibration Measurement Taken from COTS Device

Number of measurements	Vibration Magnitude (in IPS)	Vibration Phase (in Degree)
1	0.157	68.5
2	0.166	82.5

In order to compare the results, regression models are trained with raw data of the measurements. In order to train the models, 100 different measurements are sampled from a constant vibration generator lab device. After the training was completed, 33 different raw data samples were given to models to predict the vibration magnitude and phase. The result of the study is given below;

Table 6. Vibration magnitude results of the trained models

Data Number	Signal Processing	Matern 5/2 Gaussian Process Regression	Squared Exponential GPR	Rational Quadratic GPR	Linear SVM	Linear Regression	Fine Gaussian SVM
1	0.385	0.3845	0.3845	0.3845	0.3832	0.3846	0.3844
2	0.3889	0.3887	0.3887	0.3887	0.3878	0.3876	0.3875
3	0.3856	0.3853	0.3853	0.3853	0.3841	0.3865	0.3845
4	0.389	0.3915	0.3915	0.3915	0.3917	0.3935	0.3874
5	0.3821	0.3855	0.3855	0.3855	0.3844	0.3841	0.3862
6	0.3815	0.3838	0.3838	0.3838	0.3829	0.3851	0.3867
7	0.3824	0.3855	0.3855	0.3855	0.3846	0.3808	0.3869
8	0.3825	0.3842	0.3842	0.3842	0.3833	0.3847	0.3868
9	0.3828	0.3868	0.3868	0.3868	0.3859	0.3868	0.3867
10	0.3842	0.3862	0.3862	0.3862	0.3847	0.3814	0.3868
11	0.3836	0.387	0.387	0.387	0.387	0.3846	0.3871
12	0.3835	0.3869	0.3869	0.3869	0.3861	0.3836	0.3865
13	0.384	0.3862	0.3862	0.3862	0.3851	0.3873	0.3868
14	0.3836	0.3868	0.3868	0.3868	0.386	0.3843	0.3864

15	0.3832	0.3859	0.3859	0.3859	0.3851	0.3847	0.3865
16	0.3841	0.3865	0.3865	0.3865	0.3854	0.3859	0.3868
17	0.3833	0.3875	0.3875	0.3875	0.3872	0.383	0.3869
18	0.3835	0.3861	0.3861	0.3861	0.385	0.3825	0.3869
19	0.3838	0.3867	0.3867	0.3867	0.3868	0.3816	0.3871
20	0.3845	0.3871	0.3871	0.3871	0.3858	0.3844	0.3868
21	0.3847	0.3854	0.3854	0.3854	0.3847	0.3836	0.3868
22	0.3856	0.3888	0.3888	0.3888	0.3876	0.3878	0.3874
23	0.3864	0.3898	0.3898	0.3898	0.3891	0.3878	0.3873
24	0.387	0.3887	0.3887	0.3887	0.3865	0.3888	0.3874
25	0.387	0.3892	0.3892	0.3892	0.3888	0.3872	0.3872
26	0.3871	0.3899	0.3899	0.3899	0.3908	0.3916	0.3878
27	0.3872	0.3889	0.3889	0.3889	0.3888	0.3869	0.3872
28	0.3881	0.3889	0.3889	0.3889	0.3875	0.3862	0.3873
29	0.3875	0.3885	0.3885	0.3885	0.3865	0.3867	0.3872
30	0.3875	0.3898	0.3898	0.3898	0.3882	0.3893	0.3877
31	0.3879	0.3901	0.3901	0.3901	0.3906	0.3897	0.3871
32	0.3879	0.3892	0.3892	0.3892	0.3875	0.3886	0.3872
33	0.3879	0.3898	0.3898	0.3898	0.3885	0.3864	0.3876

Table 7. Vibration Phase Results of the Trained Model

Data Number	Signal Processing	Exponential GPR	Squared Exponential GPR	Rational Quadratic GPR	Matern 5/2 GPR	Medium Gaussian SVM	Ensemble Bagged Trees
1	273.1626	272.0677	271.852	271.852	271.8612	271.764	272.1001
2	276.9804	277.5151	278.3383	278.3383	278.2952	277.8863	278.8763
3	270.6296	271.7011	272.1645	272.1645	272.1169	271.6672	271.8512
4	279.5511	278.2309	278.0468	278.0468	277.9674	277.3906	277.5973
5	269.127	272.3796	272.1127	272.1127	272.065	272.1133	272.437
6	269.2714	271.6013	271.5404	271.5404	271.4342	271.0748	272.1513
7	269.4738	272.1517	271.9159	271.9159	271.8817	272.6021	274.5612
8	270.4111	272.3632	272.1138	272.1138	272.0535	271.4984	272.3901
9	272.1517	271.542	271.5396	271.5396	271.3897	271.4003	272.733
10	269.757	271.58	271.2489	271.2489	271.1412	271.8384	275.1639
11	270.3909	273.965	272.9339	272.9339	273.1164	274.2403	273.1702
12	270.9227	272.3794	272.1907	272.1907	272.1342	272.4082	273.7117
13	271.2152	271.4306	271.5516	271.5516	271.4234	271.2122	272.3331
14	271.9548	272.0812	272.0657	272.0657	271.966	271.8728	273.1894
15	272.5551	272.5851	272.4425	272.4425	272.3676	271.8668	272.4999
16	272.5441	271.5523	271.6167	271.6167	271.4895	271.6144	275.6128
17	273.2305	273.0869	272.694	272.694	272.7381	273.3504	273.2266
18	273.366	271.5446	271.5873	271.5873	271.4499	271.3047	274.5405
19	273.5273	274.1208	273.3208	273.3208	273.509	274.1132	273.7253

20	273.5038	271.6582	271.9291	271.9291	271.7778	271.3329	272.9602
21	270.5502	272.1372	272.1967	272.1967	272.0716	271.5683	272.8956
22	278.7988	276.3216	276.8981	276.8981	276.76	276.8022	278.1854
23	275.6509	276.5094	276.7086	276.7086	276.5841	276.519	277.7963
24	276.1907	276.9878	277.2623	277.2623	277.2004	276.8702	277.544
25	276.5358	276.6504	276.4354	276.4354	276.3338	276.7422	277.7938
26	277.3118	277.3081	277.4066	277.4066	277.4863	277.1829	276.9551
27	279.401	278.6897	278.2429	278.2429	278.2821	277.7171	278.6084
28	276.338	277.1326	277.5101	277.5101	277.4423	276.8235	277.6751
29	278.163	277.4387	277.9638	277.9638	277.866	277.1947	277.5127
30	279.0325	277.3911	277.2941	277.2941	277.2402	277.2633	277.9593
31	279.0475	278.4451	277.6802	277.6802	277.7391	277.7758	278.6596
32	279.0475	277.3233	278.3911	278.3911	278.2703	276.9664	278.0281
33	279.0475	277.1234	276.9896	276.9896	276.9224	277.0225	277.8487

Results show that in both methods, both magnitude and the phase of the vibration signal can be detected very precisely when predicting the lab device vibration output with the trained lab device raw data. The following study was done to predict helicopter vibration data using trained lab device data. As can be seen from the tables, training with constant vibration generator data is insufficient for predicting the helicopter vibration values. This is because the lab device generates only 0,4 IPS (+/- %10) and 275o (+/- 15o) vibration signal, and the model is trained in that range.

Table 8. Helicopter Measurement Vibration Magnitude Results Due to

Data Number	Signal Processing	Matern 5/2 Gaussian Process Regression	Squared Exponential GPR	Rational Quadratic GPR	Linear SVM	Linear Regression	Fine Gaussian SVM
1	0.1603	0.335	0.3353	0.3353	0.352	0.2552	0.3871
2	0.2	0.3356	0.336	0.336	0.349	0.2121	0.3871
3	0.1982	0.331	0.3314	0.3314	0.342	0.2089	0.3871
4	0.1924	0.3395	0.3398	0.3398	0.351	0.2379	0.3871
5	0.1664	0.3463	0.3465	0.3465	0.362	0.2562	0.3871
6	0.2271	0.3332	0.3335	0.3335	0.347	0.1644	0.3871
7	0.1699	0.3287	0.3291	0.3291	0.344	0.288	0.3871
8	0.1777	0.3321	0.3325	0.3325	0.344	0.2225	0.3871
9	0.1763	0.3403	0.3406	0.3406	0.356	0.2126	0.3871
10	0.1882	0.3364	0.3368	0.3368	0.348	0.249	0.3871
11	0.1355	0.336	0.3363	0.3363	0.352	0.216	0.3871
12	0.1469	0.3397	0.34	0.34	0.354	0.268	0.3871
13	0.1582	0.3362	0.3365	0.3365	0.349	0.2841	0.3871
14	0.1602	0.3321	0.3325	0.3325	0.35	0.2422	0.3871

2.6.1. Lab Device Data Training

Table 9. Helicopter Measurement Vibration Phase Results Due to Lab Device Data Training

Data Number	Signal Processing	Exponential GPR	Squared Exponential GPR	Rational Quadratic GPR	Matern 5/2 GPR	Medium Gaussian SVM	Ensemble Bagged Trees
1	217.51	281.5835	281.6043	281.6043	278.3061	279.0538	276.2309
2	227.96	281.7053	282.7767	282.7767	279.4892	279.0538	277.384
3	223.34	281.3627	282.1509	282.1509	278.862	279.0538	276.272
4	238.27	281.6442	283.5714	283.5714	280.6742	279.0538	277.7772
5	234.99	281.8797	283.7744	283.7744	280.9139	279.0538	276.8457
6	223.45	281.7704	283.6886	283.6886	280.4007	279.0538	277.7414
7	204.6	281.3327	281.8019	281.8019	277.9771	279.0538	276.0335
8	206.68	281.5704	282.9903	282.9903	279.9599	279.0538	277.2747
9	217.72	281.3713	282.4934	282.4934	278.7991	279.0538	276.9685
10	225.58	281.4698	283.5887	283.5887	279.9693	279.0538	277.5802
11	242.95	281.7613	282.5895	282.5895	279.4875	279.0538	276.876
12	239.12	281.8797	283.1841	283.1842	280.188	279.0538	277.1606
13	222.11	281.8278	283.2737	283.2737	280.3337	279.0538	276.2135
14	240.21	281.7427	283.0528	283.0528	279.5378	279.0538	275.5625

In order to improve the trained model, the dataset for the lab device is reduced to 50, and 19 helicopter measurements are included in the training dataset. Therefore, the training model is updated to the 69 69-dataset, including helicopter measurement data. Afterwards, newly trained models are tried for predicting helicopter data. The following table shows the results of the study.

Table 10. Helicopter Measurement Vibration Magnitude Results Due to New Trained Model Including Helicopter Data

Data Number	Signal Processing	Rational Quadratic GPR	Squared Exponential GPR	Exponential GPR	Matern 5/2 GPR	Linear SVM	Ensemble Bagged Trees
1	0.152	0.1538	0.1538	0.1764	0.1499	0.1373	0.1747
2	0.159	0.168	0.168	0.1781	0.1666	0.1635	0.1769
3	0.117	0.1543	0.1543	0.1713	0.1531	0.1538	0.1746
4	0.123	0.155	0.155	0.1697	0.1519	0.1491	0.1897
5	0.103	0.1684	0.1684	0.1776	0.1649	0.1557	0.1838
6	0.143	0.1269	0.1269	0.1581	0.125	0.1323	0.2023
7	0.136	0.1744	0.1744	0.1902	0.1717	0.1686	0.2017
8	0.12	0.1398	0.1398	0.1697	0.1368	0.1427	0.1861

Table 11. Helicopter Measurement Vibration Phase Results Due to the New Trained Model Including Helicopter Data

Data Number	Signal Processing	Matern 5/2 GPR	Quadratic SVM	Squared Exponential GPR	Rational Quadratic GPR	Linear SVM	Exponential GPR
1	64.16	96.0429	124.8237	111.7863	102.8103	130.571	83.7206
2	66.79	61.3822	77.4088	66.83	64.3869	57.4755	67.8963
3	74.72	52.1545	75.4194	53.5759	53.0118	65.2587	66.6897
4	51.59	81.443	112.0097	93.351	86.5453	120.824	81.9588
5	85.98	85.6498	124.7238	98.9884	91.4014	134.6506	84.3849
6	-2	65.4232	67.1214	68.0141	67.1388	78.8146	78.5903
7	57.83	120.4378	136.1189	135.2336	126.118	157.1943	97.8218
8	64.5	81.8943	120.9024	90.5852	85.7738	120.1917	84.845

3. Results and Discussion

One may say that the results are improved when helicopter data is included in the training dataset. However, the precision of the prediction is still not sufficient. In order to improve the model's precision, the dataset should be expanded with more helicopter vibration measurements.

The whole idea for detecting the vibration level of the system is to compensate for it. In other words, eliminates the vibration from the system. In rotating systems, vibration is caused by the tilt of the rotating system axis. This tilted axis occurs in helicopter blades when the reciprocal blade weights are mismatched. In order to get matched blade weights, balance charts are used for helicopters. This chart's data depends upon helicopter types and is given by the helicopter manufacturers. Simply, charts guide technicians to decrease the vibration levels by telling them to add or remove weights to the blades, after vibration signal measurements are done. The measured vibration data are placed into balance chart graphs according to the IPS and the phase value. After the placement is done, the chart axis guides the technician in modifying the weight of the blade. A representative figure of a helicopter balance chart is given below;

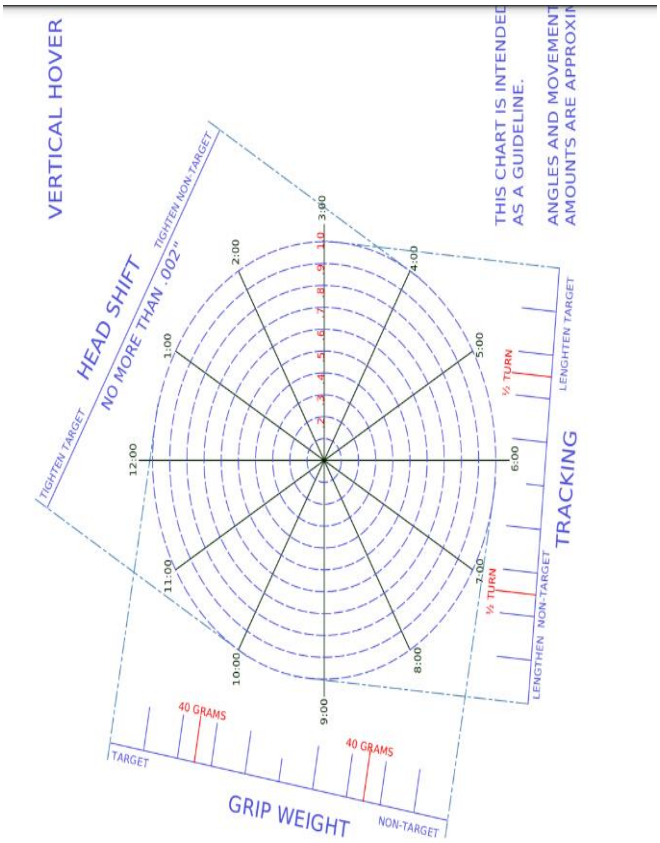

Fig. 20 Balance Chart of a Helicopter

Finally, the comparison of several specifications between the designed FTI system and the COTS device that is used in the experimental setup is given below.

Table 12. Specification Comparison Between COTS Device and Designed FTI System

	Designed FTI System	COTS Device
Dimensions	25 x 10.5 x 11 cm	27.4 x 19.1 x 10.2 cm
Weight	2.275 kg	3.22 kg
Frequency Range	2 Hz - 10 kHz	3.33 Hz - 10 kHz
Memory	8GB internal, 512 GB on User PC	2 MB SRAM, 1 MB Flash EPROM
Channel	24 Channels and Extensible	36 Channels
Power Range	18-40 VDC (28 VDC Nominal)	12-28 VDC (28 VDC Nominal)
Temperature Range	(-40°C to +85°C)	(-40°C to +55°C)

4. Conclusion

The Conclusions section should clearly explain the main findings and implications of the work, highlighting its importance and relevance.

Within the scope of this thesis, an FTI system is designed, vibration signals are analyzed, and the vibration level of helicopters is measured. The studies that are conducted in this context can be summarized as follows:

- In order to design an FTI system, requirements are issued. In light of derived requirements, an FTI system is designed that consists of modules: a power module, controller module, analog input module and backplane module that combines all modules.
- A system architecture is designed for a data acquisition system in order to communicate analog input modules with the controller module through the SPI interface. Also, a gigabit Ethernet interface is implemented to communicate with the user's PC. Finally, another SPI interface for the ADC and configuration modules for analog input module is implemented in VHDL.
- A signal processing algorithm was developed and implemented to designed the FTI system. In order to extract the vibration magnitude from the velocimeter measurements, an FFT module is implemented in the algorithm. Digital filters are designed and implemented for noisy data for phase extraction. A constant vibration generator device is used to verify the algorithm. After that, the algorithm and the designed device are verified on a helicopter using another COTS vibration analyzer.
- Regression models are trained to predict vibration magnitude and phase values by using constant vibration generator device measurements. Afterwards, the trained model is used to predict helicopter vibration data. However, the range of the trained data was limited due to constant vibration, so the trained model was insufficient for predicting helicopter vibration values. In order to

improve the model, helicopter measurements are included in the training dataset. Simulation results show that predictions are improved but still not very effective.

As a result, the vibration magnitude and phase of the helicopters were determined using signal processing algorithms, and the results of this study are promising. For the machine learning algorithms, conducted experiments show that the training datasets should be expanded with more velocimeter data sampled from a helicopter to use the trained models in helicopter studies.

References

[1] Donald R. Houser, and Michael J. Drosjack, *Vibration Signal Analysis Techniques*, Ohio State University, 1973. [Google Scholar] [Publisher Link]

[2] Biji Mathew et al., "A Review on Vibration Analysis of Helicopter Rotor Blade," *International Journal for Research in Applied Science and Engineering Technology*, vol. 10, no. 2, pp. 1363-1369, 2022. [CrossRef] [Google Scholar] [Publisher Link]

[3] Curtiss-Wright, Data Acquisition Systems. [Online]. Available: https://www.curtisswrightds.com/products/flight-test/data-acquisition

[4] Traco Power, TEN20WIN Series, 20Watt, 2025. [Online]. Available: https://www.tracopower.com/ten20win-datasheet

[5] Analog Devices, Analog Filter Wizard. [Online]. Available: https://tools.analog.com/en/filterwizard/

[6] Texas Instruments, Quad/Octal, Simultaneous Sampling, 24-Bit Analog-to-Digital Converters. https://www.ti.com/lit/ds/symlink/ads1274.pdf?ts=1737971409427&ref_url=https%253A%252F%252Fwww.google.com%252F

[7] Zhou Wang, and Alan C. Bovik, "Mean Squared Error: Love it or Leave it? A New Look at Signal Fidelity Measures," *IEEE Signal Processing Magazine*, vol. 26, no. 1, pp. 98-117, 2009. [CrossRef] [Google Scholar] [Publisher Link]

[8] Dulakshi Santhusitha, and Kumari Karunasingha, "Root Mean Square Error or Mean Absolute Error? Use Their Ratio as Well," *Information Sciences*, vol. 585, pp. 609-629, 2022. [CrossRef] [Google Scholar] [Publisher Link]

[9] Vikramaditya Jakkula, "*Tutorial on Support Vector Machine*," School of EECS, Washington State University, Pullman, vol. 37, 2006. [Google Scholar] [Publisher Link]

[10] Barry de Ville, "Decision Trees," *Wire Computational Statistics*, vol. 5, no. 6, pp. 448-455, 2013. [CrossRef] [Google Scholar] [Publisher Link]

[11] Eric Schulz, Maarten Speekenbrink, and Andreas Krause, "A Tutorial on Gaussian Process Regression: Modelling, Exploring, and Exploiting Functions," *Journal of Mathematical Psychology*, vol. 85, pp. 1-16, 2018. [CrossRef] [Google Scholar] [Publisher Link]

[12] Martin Sewell, "Ensemble Learning," UCL Department of Computer Science, 2011. [Google Scholar] [Publisher Link]